

Relativistic stars in $f(R)$ and scalar-tensor theories

Eugeny Babichev^{a,b}, David Langlois^{a,c}

^a APC, UMR 7164 (CNRS-Université Paris 7), 10 rue Alice Domon et Léonie Duquet, 75205 Paris Cedex 13, France

^b Institute for Nuclear Research of the Russian Academy of Sciences,
60th October Anniversary Prospect, 7a, 117312 Moscow, Russia and

^c IAP (Institut d'Astrophysique de Paris), 98bis Boulevard Arago, 75014 Paris, France

(Dated: February 23, 2019)

We study relativistic stars in the context of scalar tensor theories of gravity that try to account for the observed cosmic acceleration and satisfy the local gravity constraints via the chameleon mechanism. More specifically, we consider two types of models: scalar tensor theories with an inverse power law potential and $f(R)$ theories. Using a relaxation algorithm, we construct numerically static relativistic stars, both for constant energy density configurations and for a polytropic equation of state. We can reach a gravitational potential up to $\Phi \sim 0.3$, even in $f(R)$ theories with an “unprotected” curvature singularity. However, we find static configurations only if the pressure does not exceed three times the energy density, except possibly in a limited region of the star (otherwise, one expects tachyonic instabilities to develop). This constraint is satisfied by realistic equations of state for neutron stars.

I. INTRODUCTION

One of the most challenging tasks for cosmology and fundamental physics today is to try to understand the apparent acceleration of the Universe. Beyond the minimal assumption of a pure cosmological constant, two main approaches have been explored. The first one consists in assuming some unknown form of matter, called *dark energy*, characterized by an equation of state $P \simeq -\rho$. The second approach is more radical, as it tries to explain the present observations as the manifestation of a modified theory of gravity, which mimicks general relativity on solar system scales, but significantly deviates from it on cosmological scales.

It turns out that it is rather difficult to construct a theory of gravity that, while being internally consistent, can account for the cosmological observations and be compatible with the present gravity constraints deduced from laboratory experiments and from solar and astrophysical systems. A class which has attracted a lot of attention is the so-called $f(R)$ gravity theories where the standard Einstein-Hilbert gravitational Lagrangian, proportional to the scalar curvature R , is replaced by a function of R while the matter part of the Lagrangian is left unchanged (see e.g. [1] for a recent review). After several detours, it has been realized that viable $f(R)$ theories must satisfy stringent conditions in order to avoid instabilities and to satisfy the present laboratory and solar system constraints, and a few models have been carefully constructed to meet these requirements [2, 3, 4].

To explore the full viability of these theories, it is important to go one step further by studying their behaviour in the strong gravity regime, such as reigns in the core of the most relativistic stars, namely neutron stars. In this context, it has been claimed in [5, 6] that very relativistic stars do not exist in the models [2, 3, 4] because of the presence of an easily accessible singularity. In a recent work [7], we have shown that this claim does not hold by constructing numerically static relativistic stars. Note that relativistic stars have also been studied in [8] but within different $f(R)$ models.

$f(R)$ models can also be seen as a subclass of scalar-tensor theories. In particular, viable $f(R)$ models rely on the so-called chameleon mechanism. For this reason, it is interesting to extend the study of relativistic stars to chameleon models. In this work, we show that the behaviour of chameleon and $f(R)$ models is quite similar. In particular, in both cases, the scalar field in the innermost part of the star sticks to the minimum of its effective potential (if this minimum exists). If the equation of state is such that $\rho - 3P < 0$, which occurs in the central part of highly relativistic constant energy density stars, then there is no minimum. As we show here, it is nevertheless possible to construct numerically static stars, up to some critical value of the central energy density. We believe that this is due to tachyonic instabilities, associated with a negative effective squared mass, which develop and prevent the existence of a static star configuration. However, this problem does not apply to realistic neutron stars: although there is a large uncertainty on the equation of state deep inside a neutron star, the equations of state that have been proposed in the literature verify $\rho - 3P > 0$ throughout the star. To construct a simple approximation of a realistic neutron star, we have used a polytropic equation of state.

Although, according to our previous work [7] and the present one, the singularity of the models [2, 3, 4] does not seem so far to be an obstacle for relativistic stars, it appears to be problematic for cosmology [5]. This has motivated

the construction of regularized versions of these models by adding for instance an extra R^2 term [4, 9, 10, 11, 12]. A more sophisticated model was also proposed recently in [13]. We will consider these “cured” $f(R)$ theories and compare their behaviour in relativistic stars with their “singular” counterparts.

This paper is organized as follows. In the next section, we derive the main equations governing static and spherically symmetric configurations in scalar-tensor theories. Section 3 is devoted to relativistic stars in chameleon models. We then consider, in Section 4, the $f(R)$ models, including the “cured” models that have been recently been introduced to solve the cosmological singularity problem of some of these models. We finally conclude in Section 6.

II. STATIC AND SPHERICALLY SYMMETRIC EQUATIONS

In the present work, we consider models characterized by an action of the form

$$S = \int d^4x \sqrt{-g} \left[\frac{M_P^2}{2} R - \frac{1}{2} (\nabla\phi)^2 - V(\phi) \right] + S_m(\Psi_m; \tilde{g}_{\mu\nu}), \quad (1)$$

with $M_P^2 \equiv 8\pi G$, and where the matter (i.e. the fields Ψ_m) is minimally coupled to the metric

$$\tilde{g}_{\mu\nu} = \Omega^2(\phi) g_{\mu\nu}.$$

For simplicity, we consider only couplings of the form

$$\Omega = \exp\left(Q \frac{\phi}{M_P}\right), \quad (2)$$

where Q is a constant, although more general functions can have interesting effects (such as the spontaneous scalarization discovered in [14] for coupling functions of the form $\ln \Omega = \beta\phi^2/2$ with $\beta < 0$).

Viable scalar-tensor theories are severely restricted by the present constraints on gravity, coming from laboratory experiments, solar system and binary pulsar tests. For example, deviations from General Relativity (GR) can be parametrized by the post-Newtonian parameters $(\tilde{\beta} - 1)$ and $(\tilde{\gamma} - 1)$. For the coupling (2), one finds (see e.g. [15]¹)

$$\tilde{\beta} - 1 = 0, \quad \tilde{\gamma} - 1 = -4 \frac{Q^2}{1 + 2Q^2}.$$

The present constraint, inferred from solar system tests, is [16]

$$|\tilde{\gamma} - 1| \lesssim 2 \times 10^{-5}.$$

The binary pulsars also give a similar constraint, but which is so far weaker than the solar system constraint in our case². The above constraint suggests that scalar tensor theories of gravity can be viable only for very small couplings between ordinary matter and the scalar field.

However, this constraint can be evaded if the scalar field is endowed with a potential such that its effective mass becomes large in the presence of matter. This is the so-called chameleon effect [18, 19]. As a consequence of this effect, the “bare” coupling constant Q is replaced by an effective coupling Q_{eff} which can be strongly suppressed, i.e. such that $|Q_{\text{eff}}| \ll |Q|$. The purpose of this paper is to study relativistic stars in this type of gravity. This also applies to $f(R)$ theories, which can be recast in the form of scalar tensor theories with $Q = -1/\sqrt{6}$, leading to the unacceptable value $\tilde{\gamma} = 1/2$ [20]. Therefore, these theories can be considered as viable if the corresponding potential allows for a chameleon effect [21, 22, 23].

A. Links between the Jordan and Einstein frames

The action (1) is defined in the Einstein frame, where gravity is described by the usual Einstein-Hilbert term for the metric $g_{\mu\nu}$. This metric differs from the metric $\tilde{g}_{\mu\nu}$, defined in the Jordan frame, which is directly felt by the

¹ Note that our ϕ is related to the scalar field φ defined in [15] by $\phi = \sqrt{2}M_P\varphi$ and therefore their α corresponds to $\alpha = \sqrt{2}Q$.

² This can be seen on the figure 11 of the very recent lecture notes by G. Esposito-Farese [17]. For models with a coupling of the form (2), the parameter space is restricted to the vertical axis $\beta_0 = 0$ where, so far, the solar system constraints turn out to be more stringent.

matter. As a consequence, one must be careful to specify the metric with respect to which various quantities are defined. For example, the energy-momentum tensor, defined in the Jordan frame and denoted $\tilde{T}_{\mu\nu}$, is related to the energy-momentum tensor defined in the Einstein frame, $T_{\mu\nu}$, by

$$\tilde{T}_{\nu}^{\mu} = \Omega^{-4} T_{\nu}^{\mu},$$

so that, for a perfect fluid, we have

$$\rho = \Omega^4 \tilde{\rho}, \quad P = \Omega^4 \tilde{P}.$$

The equation of state will always be specified in the Jordan frame. When $|Q\phi/M_P| \ll 1$, as will be the case for our relativistic stars, the numerical values for the energy density and the pressure are essentially the same in the two frames.

B. Equations of motion

In Einstein's frame, the equations of motion are given by

$$G_{\mu\nu} = M_P^{-2} \left[T_{\mu\nu}^{(m)} + \partial_{\mu}\phi\partial_{\nu}\phi - \frac{1}{2}g_{\mu\nu}\partial^{\sigma}\phi\partial_{\sigma}\phi - Vg_{\mu\nu} \right], \quad (3)$$

$$\nabla_{\sigma}\nabla^{\sigma}\phi = -\frac{dV}{d\phi} - \frac{\Omega'}{\Omega}T^{(m)}, \quad (4)$$

where $G_{\mu\nu} \equiv R_{\mu\nu} - (1/2)Rg_{\mu\nu}$ is the Einstein tensor, $T_{\mu\nu}^{(m)}$ is the energy-momentum tensor for the fluid matter of the star (i.e. does not include the scalar field) and

$$T^{(m)} \equiv g^{\mu\nu}T_{\mu\nu}^{(m)} = -\rho + 3P$$

is its trace.

We now consider a static and spherically symmetric geometry, with metric

$$ds^2 = -e^{\nu}dt^2 + e^{\lambda}dr^2 + r^2(d\theta^2 + \sin^2\theta d\phi^2).$$

Introducing the radial function $m(r)$ so that

$$e^{-\lambda} \equiv 1 - 2m/r,$$

the time and radial components of Einstein's equations (3) yield, respectively,

$$m' = \frac{r^2}{2M_P^2} \left[\Omega^4 \tilde{\rho} + \frac{1}{2}e^{-\lambda}\phi'^2 + V(\phi) \right], \quad (5a)$$

$$\nu' = e^{\lambda} \left[\frac{2m}{r^2} + \frac{r}{M_P^2} \left(\frac{1}{2}e^{-\lambda}\phi'^2 - V(\phi) \right) + \frac{r\Omega^4 \tilde{P}}{M_P^2} \right], \quad (5b)$$

where one recognizes, inside the brackets of the first equation, the total energy density, which includes the fluid energy density (defined in the Einstein frame) as well as the gradient and potential energies of the scalar field.

Instead of the angular component of Einstein's equations, it is convenient to use the conservation of the fluid energy-momentum, which has the standard form,

$$\tilde{\nabla}_{\mu}\tilde{T}_{(m)\nu}^{\mu} = 0,$$

in the Jordan frame, where the matter is minimally coupled. This gives

$$\tilde{P}' = -\frac{1}{2}(\tilde{\rho}' + \tilde{P}') \left(\nu' + 2\frac{\Omega'}{\Omega}\phi' \right). \quad (6)$$

The last equation is provided by the Klein-Gordon equation, Eq. (4), for the scalar field,

$$\phi'' + \left(\frac{2}{r} + \frac{1}{2}(\nu' - \lambda') \right) \phi' = e^{\lambda} \left[\frac{dV}{d\phi} + \Omega^3 \Omega' (\tilde{\rho} - 3\tilde{P}) \right]. \quad (7)$$

Finally, an equation of state,

$$\tilde{P} = \tilde{P}(\tilde{\rho}), \quad (8)$$

closes the system of equations (5a), (5b), (6) and (7).

C. Constant energy density stars

In general relativity, one can solve analytically the profile of a relativistic star by assuming that the energy density is constant,

$$\rho = \rho_0.$$

Using (5a) in the GR limit, which corresponds to $\phi = 0$ and $V(\phi) = 0$, this implies

$$m(r) = \frac{\rho_0 r^3}{6M_P^2}.$$

Substituting in the Tolman-Oppenheimer-Volkov equation

$$P' = -\frac{\rho + P}{r^2(1 - 2m/r)} \left[m + \frac{r^3 P}{2M_P^2} \right],$$

which follows from (6) and (5b) in the GR limit, one finds, after integration, that the pressure profile is given by

$$P(r) = \rho_0 \frac{\left(1 - \frac{2GM_*}{r_*}\right)^{1/2} - \left(1 - \frac{2GM_* r^2}{r_*^3}\right)^{1/2}}{\left(1 - \frac{2GM_* r^2}{r_*^3}\right)^{1/2} - 3\left(1 - \frac{2GM_*}{r_*}\right)^{1/2}} \quad (9)$$

where r_* is the radius of the star and $M_* \equiv 4\pi\rho_0 r_*^3/3$ its mass.

We can use the above analytical results to compute the trace of the energy momentum-tensor, which is the quantity that couples directly to the scalar field in its equation of motion. The relation (9) implies

$$\rho - 3P = \rho_0 \frac{4\left(1 - \frac{2GM_* r^2}{r_*^3}\right)^{1/2} - 6\left(1 - \frac{2GM_*}{r_*}\right)^{1/2}}{\left(1 - \frac{2GM_* r^2}{r_*^3}\right)^{1/2} - 3\left(1 - \frac{2GM_*}{r_*}\right)^{1/2}}.$$

Since this is a function that grows with increasing r , its minimal value is at the center of the star and is given by

$$\rho_c - 3P_c = \rho_0 \frac{4 - 6(1 - 2\Phi_*)^{1/2}}{1 - 3(1 - 2\Phi_*)^{1/2}}, \quad \Phi_* \equiv \frac{GM_*}{r_*},$$

where Φ_* is the gravitational potential at the star surface. Therefore, whenever the compactness of the star is higher than the critical value

$$\Phi_* = \frac{5}{18} \simeq 0.28, \quad (10)$$

the quantity $\rho - 3P$ becomes negative in the most central layers of the star. As we will see later, the sign of $\rho - 3P$ is crucial to understand the behaviour of the scalar field inside the star and can have drastic implications concerning the stability of the scalar field. Note that this critical value was also pointed out in [24]. Note also that although our derivation above applies only to constant energy density stars in pure general relativity, it remains a good approximation for the stars we consider because the backreaction of the scalar field on the star profile is very small.

D. More realistic equation of state

Although analytically simple, a constant energy density star is not a very realistic substitute for a real neutron star. Since the equation of state deep inside a neutron star is still unknown, we use in this paper a polytropic equation of state, which remains simple and is believed to represent a reasonable approximation for a real neutron star. It is given by

$$\tilde{\rho}(\tilde{n}) = m_B \left(\tilde{n} + K \frac{\tilde{n}^2}{n_0} \right), \quad \tilde{P}(\tilde{n}) = K m_B \frac{\tilde{n}^2}{n_0}, \quad (11)$$

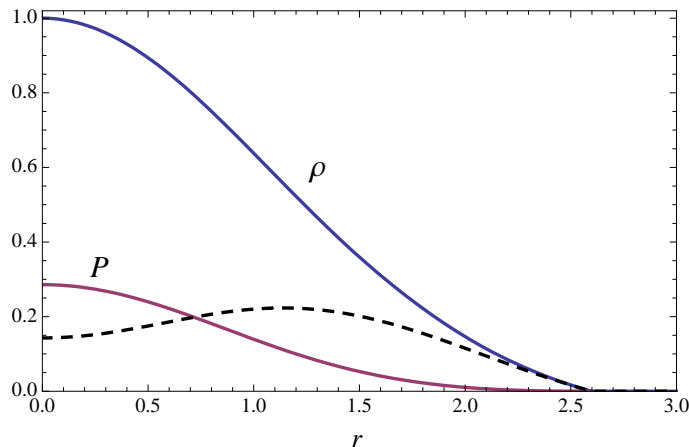


FIG. 1: Energy density $\tilde{\rho}$ (solid blue line), pressure \tilde{P} (solid purple line) and the combination $\tilde{\rho} - 3\tilde{P}$ (black dotted line), in units of the central density ρ_c , as functions of the radial coordinate r (in units of $M_P \tilde{\rho}_c^{-1/2}$).

with $m_B = 1.66 \times 10^{-27}$ kg, $n_0 = 0.1 \text{ fm}^{-3}$ and $K = 0.1$. We take for the central particle number density the value $\tilde{n}_c = 0.4 \text{ fm}^{-3}$, which corresponds to a central energy density $\tilde{\rho}_c = 9.296 \times 10^{17} \text{ kg/m}^3$ and a gravitational potential $|\Phi_*| \simeq 0.25$. This example thus describes a fairly relativistic star and we are going to use it to study relativistic stars in both chameleon and $f(R)$ models.

In Fig. 1, we plot the radial profile of the energy density and of the pressure. As can be seen in the same figure, the quantity $\tilde{\rho} - 3\tilde{P}$ remains positive throughout the star. The same holds for other realistic equations of state that have been proposed in the literature (see e.g. [25] and references therein for a discussion on the equations of state of neutron stars). Interestingly, $\tilde{\rho} - 3\tilde{P}$ is not a monotonous function of the radius in the example we have chosen. We will see that this has a visible influence on the profile of the scalar field inside the star.

E. Effective potential

Assuming some configuration for the relativistic star and ignoring any backreaction of the scalar field on this configuration, it is useful to interpret the right hand side of the Klein-Gordon equation (7), up to the metric component e^λ , as the derivative of an effective potential defined by

$$V_{\text{eff}} = V + \frac{1}{4} \Omega^4 (\tilde{\rho} - 3\tilde{P}). \quad (12)$$

Consequently, a local extremum of the potential is characterized by the condition

$$\frac{dV_{\text{eff}}}{d\phi} = \frac{dV}{d\phi} + \frac{Q}{M_P} e^{4Q\phi/M_P} (\tilde{\rho} - 3\tilde{P}) = 0. \quad (13)$$

A solution of the above equation, if it exists, corresponds to a minimum of the potential if the effective squared mass

$$m_{\text{eff}}^2 \equiv \frac{d^2 V_{\text{eff}}}{d\phi^2} = \frac{d^2 V}{d\phi^2} + 4 \frac{Q^2}{M_P^2} e^{4Q\phi/M_P} (\tilde{\rho} - 3\tilde{P})$$

is positive. It is thus manifest that the quantity $\tilde{\rho} - 3\tilde{P}$ plays a crucial rôle in the overall sign of m_{eff}^2 , with consequences for the stability of the star, which we discuss just below.

F. Stability

Although we have not performed a detailed stability analysis of our star configurations, it is possible to discuss qualitatively their stability with simple arguments. Since the effect of the backreaction of the scalar field on the star

profile is small, we simply consider the perturbations of the scalar field in the background geometry defined by the unperturbed star. Decomposing the perturbations into spherical harmonics,

$$\delta\phi(t, r, \theta, \phi) = \sum \delta\phi_{lm}(t, r) Y_{lm}(\theta, \phi),$$

one finds that each mode verifies the equation

$$\delta\ddot{\phi} - e^{\nu-\lambda} \left[\delta\phi'' + \left(\frac{\nu' - \lambda'}{2} + \frac{2}{r} \right) \delta\phi' \right] + e^\nu \left[\frac{l(l+1)}{r^2} + m_{\text{eff}}^2 \right] \delta\phi = 0.$$

Using a Fourier decomposition in time, and denoting the frequency ω , the above equation of motion leads to a dispersion relation of the form

$$\omega^2 \simeq k^2 + m_{\text{eff}}^2,$$

where k^{-1} is the typical lengthscale of variation of the scalar field. One can write $k = \alpha r_*^{-1}$, where α is typically bigger than 1 but not very much, in the situations we consider. Let us also assume that the dominant contribution to m_{eff}^2 comes from the matter part. Concentrating on the radial modes (which are potentially more dangerous), we find that the configuration is stable if,

$$\omega^2 \simeq \frac{\alpha^2}{r_*^2} + 4 \frac{Q^2}{M_P^2} \tilde{\rho}_* (1 - 3w) > 0,$$

where

$$w \equiv \tilde{P}/\tilde{\rho}.$$

Substituting $\tilde{\rho}_* \sim M_*/r_*^3$ and $\Phi_* \sim M_*/(M_P^2 r_*)$ leads to the condition

$$(1 - 3w)\Phi_* \gtrsim -1,$$

where the right hand side is some constant, but typically of order -1 . According to this relation, obtained in a very crude way, one expects instabilities to appear whenever the equation of state is such that $1 - 3w < 0$ and the star is very compact so that Φ_* is a significant fraction of one. This is precisely the situation which one encounters for very massive stars with constant energy density, where $w > 1/3$ in the central region.

G. Numerical procedure

We now present how we proceed numerically. As a first step, it is convenient to rescale the various quantities involved and to work directly with dimensionless quantities. Let us thus introduce the following rescaled variables

$$r = r_0 \xi, \quad \phi = M_0 \hat{\phi}, \quad V = \frac{M_0^2}{r_0^2} \hat{V}, \quad \tilde{\rho} = \frac{M_1^2}{r_0^2} \hat{\rho}, \quad \tilde{P} = \frac{M_1^2}{r_0^2} \hat{P}, \quad (14)$$

where r_0^{-1} , M_0 , M_1 are parameters of dimension of mass, which are so far arbitrary. Substituting the above rescalings (14) in the equations of motion (5a), (5b), (6) and (7), we obtain the following system of equations,

$$\frac{2\hat{\mathcal{M}}'}{\xi^2} = \epsilon_1^2 \hat{\rho} e^{4Q\epsilon_0 \hat{\phi}} + \epsilon_0^2 \left(\frac{1}{2} e^{-\lambda} \hat{\phi}'^2 + \hat{V} \right), \quad (15a)$$

$$\nu' e^{-\lambda} = \frac{2\hat{\mathcal{M}}}{\xi^2} + \epsilon_1^2 \xi \hat{P} e^{4Q\epsilon_0 \hat{\phi}} + \epsilon_0^2 \xi \left(\frac{1}{2} e^{-\lambda} \hat{\phi}'^2 - \hat{V} \right), \quad (15b)$$

$$\hat{P}' = -\frac{1}{2} (\hat{\rho} + \hat{P}) (\nu' + 2Q\epsilon_0 \hat{\phi}'), \quad (15c)$$

$$0 = \hat{\phi}'' + \left(\frac{2}{\xi} + \frac{1}{2} (\nu' - \lambda') \right) \hat{\phi}' - e^\lambda \left[\frac{d\hat{V}}{d\hat{\phi}} + \frac{\epsilon_1^2}{\epsilon_0} Q e^{4Q\epsilon_0 \hat{\phi}} (\hat{\rho} - 3\hat{P}) \right], \quad (15d)$$

where we have used the particular coupling (2) and introduced the notations,

$$\hat{\mathcal{M}} \equiv \frac{1}{2} \xi (1 - e^{-\lambda}), \quad \epsilon_0 \equiv \frac{M_0}{M_P}, \quad \epsilon_1 \equiv \frac{M_1}{M_P}.$$

In the following, we will always take $\epsilon_1 = 1$.

Meanwhile the equation of state (8) transforms into

$$\hat{P} = \hat{P}(\hat{\rho}). \quad (16)$$

For the polytropic equation of state Eq.(11), with $\tilde{n}_c = 0.4 \text{ fm}^{-3}$, we will always choose $r_0 = M_P \tilde{\rho}_c^{-1/2}$, so that

$$\hat{\rho}_c = 1 \quad (\text{polytropic star}).$$

The equation of state Eq.(11) then becomes, in these rescaled units,

$$\hat{\rho} = \hat{P} + 2\sqrt{\frac{\hat{P}}{2.24}} \iff \hat{P} = \frac{1}{2.24} \left(\sqrt{1 + 2.24\hat{\rho}} - 1 \right)^2, \quad (17)$$

with the rescaled central pressure $\hat{P}_c \simeq 0.286$. Since the neutron star is a highly relativistic object, this choice entails that the radius of the star in rescaled units is of order one, $\xi_* \equiv r_*/r_0 \sim 1$.

Since we study static configurations, a natural way to proceed with numerics is to use a relaxation algorithm. In the following calculations the relaxation parameter will be taken to vary with the iteration number (typically between 10^{-3} and 1), in order to ensure the convergence of the algorithm and to minimize the number of iterations. We have used a non-homogenous grid, usually between 1000 and 6000 points. The details of the grid depend on the model under consideration and its parameters. Normally the grid is chosen so that the points of the grid are highly concentrated in the particular region inside the star where the solution varies rapidly. Such a choice of inhomogeneous grid allows us to numerically resolve potentially problematic regions.

Let us finally discuss the boundary conditions. The system (15), which includes three first-order differential equations and one second-order differential equation, requires five boundary conditions. Some of them are defined at the center of the star, at $\xi = 0$, while the remaining ones are specified far from the star, at some point $\xi = \xi_2$. The boundary conditions for the metric components and the scalar field are

$$\hat{\mathcal{M}}(0) = 0, \quad \nu(\xi_2) = 0, \quad \hat{\phi}'(0) = 0, \quad \hat{\phi}(\xi_2) = \hat{\phi}_\infty. \quad (18)$$

The boundary conditions for $\hat{\mathcal{M}}$ and $\hat{\phi}$ at the center just follow from the requirement of regularity at $\xi = 0$. The condition on ν is in fact arbitrary, since only ν' enters (15) but not ν itself: our choice corresponds to defining the time coordinate as the proper time of a static observer at ξ_2 . The “asymptotic” value $\hat{\phi}_\infty$ corresponds to the minimum of the effective potential \hat{V}_{eff} far from the star³. Finally, the boundary condition for the pressure is

$$\hat{P}(0) = \hat{P}_c \quad \text{or} \quad \hat{P}(\xi_2) = \hat{P}_\infty,$$

depending on the problem: for a constant-density star it is convenient to choose $\hat{P}(\xi_2) = -\hat{\rho}_\infty$ so that the solution is asymptotically de Sitter, while for the polytropic equation state, the pressure at the origin is fixed⁴.

III. CHAMELEON

A. Description of the models

In this section we consider chameleon scalar-tensor theories, introduced in [18, 19]. In these models, the effective mass of the scalar field becomes important inside matter so that the usual constraints on fifth-force interactions are evaded. To illustrate the behaviour of a chameleon field in a relativistic star, we will concentrate on a specific model, but our results should remain qualitatively valid for other models.

We will consider the action (1) with the potential

$$V(\phi) = \frac{\mu^5}{\phi},$$

³ Some situations require a more precise boundary condition, in which case the exact value of ϕ at ξ_2 can be deduced from the asymptotic behaviour of the scalar field at large distances, which can be computed analytically.

⁴ In this case we also obtain asymptotically de Sitter solution.

where μ is a mass parameter. We will also assume that $Q > 0$.

If $Q\phi/M_P \ll 1$, which will be true for our configurations, the scalar field value corresponding to the minimum of the effective potential (12) is given by

$$\phi_{\min} = \sqrt{\frac{M_P \mu^5}{Q(\tilde{\rho} - 3\tilde{P})}}.$$

Note that this is defined only if $\tilde{\rho} - 3\tilde{P} > 0$. Therefore, there is no local minimum at the center of a constant energy density star with $\Phi_* > 5/18$.

For our numerical study, we have chosen M_0 , i.e. ϵ_0 , such that the asymptotic value of the scalar field is normalized to a value of order 1. More precisely, we take

$$M_0 = \sqrt{\frac{M_P \mu^5}{Q\tilde{\rho}_\infty}} \quad \Rightarrow \quad \epsilon_0 = \sqrt{\frac{\mu^5}{QM_P\tilde{\rho}_\infty}}$$

where $\tilde{\rho}_\infty$ is the asymptotic energy density, so that the local minimum is given by

$$\hat{\phi}_{\min} = \sqrt{\frac{\rho_\infty}{(1 - 3w)\rho}},$$

in rescaled units. Asymptotically, one thus finds $\hat{\phi}_\infty = 1/\sqrt{1 - 3w_\infty} = 1/2$ (for $w_\infty = -1$).

As for the parameter r_0 , it is convenient to choose it of the order of the star radius. In the case of the polytropic equation of state, we take $r_0 = M_P \tilde{\rho}_c^{-1/2}$, so that $\hat{\rho}_c = 1$, as mentioned earlier. For the constant energy density stars, we will adopt the same prescription for a reference star characterized by $\Phi_* = 0.165$. We will then compare this star to other stars, with the same radius but different central densities, by keeping r_0 fixed but by allowing the rescaled central density $\hat{\rho}_c$ to vary.

The rescaled potential can be written in the form

$$\hat{V} = \frac{v_0}{\hat{\phi}}, \quad v_0 = \frac{Q}{\epsilon_0} \hat{\rho}_\infty. \quad (19)$$

In rescaled units, taking $\epsilon_1 = 1$, the effective potential is thus

$$\hat{V}_{\text{eff}} = \frac{v_0}{\hat{\phi}} + \frac{1}{4\epsilon_0^2} e^{4Q\epsilon_0\hat{\phi}} (\hat{\rho} - 3\hat{P}). \quad (20)$$

while the corresponding effective squared mass is

$$\hat{m}_{\text{eff}}^2 = \frac{2v_0}{\hat{\phi}_{\min}^3} + 4Q^2 e^{4Q\epsilon_0\hat{\phi}_{\min}} (\hat{\rho} - 3\hat{P}). \quad (21)$$

Let us estimate the order of magnitude of the above parameters. A typical value for the density inside neutron stars is $\rho_c \sim 10^{15} \text{g/cm}^3$, whereas the asymptotic density is $\rho_\infty \sim 10^{-24} \text{g/cm}^3$, corresponding to the galactic density. The chameleon parameter μ is of the order of 10^{-3} . This leads to tiny values for our dimensionless parameters: $\epsilon_0 \sim 10^{-19}$ and $v_0 \sim 10^{-21}$. These realistic parameters are too small for the numerical precision that can be reached in practice and we have used parameters that are much bigger.

Asymptotically, the expression yields (21) the tiny value

$$m_{\text{eff},\infty}^2 \simeq 2v_0(1 - 3w_\infty)^{3/2},$$

where the second term is negligible for $\epsilon_0 \ll 1$. By contrast, at the center of the star, the minimum is extremely small,

$$\hat{\phi}_{\min,c} = \sqrt{\frac{v_0\epsilon_0}{Q(1 - 3w_c)}},$$

while the effective mass becomes huge

$$m_{\text{eff},c}^2 \simeq 2\sqrt{\frac{Q^3(1 - 3w_c)^3}{v_0\epsilon_0^3}}.$$

One can thus expect that the scalar field configuration will follow its local minimum (when it is defined) in the denser regions of the star.

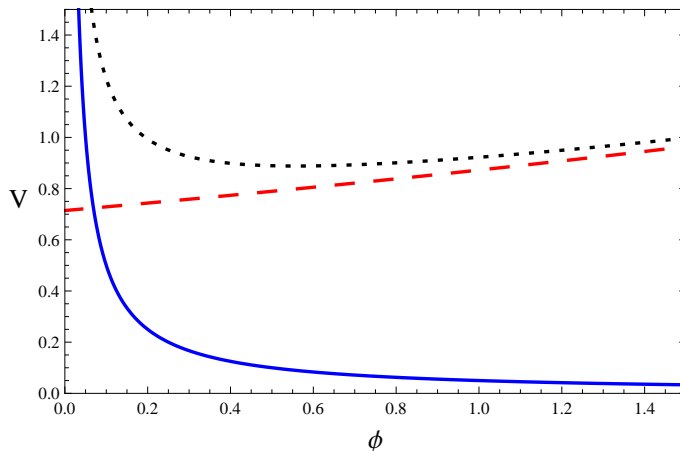


FIG. 2: The rescaled bare potentials (19), shown by solid blue, the matter part of the effective potential, shown by dashed red, and the effective potential for the chameleon model (20), shown by dotted black line. The parameters are chosen as follows, $Q = 1$, $v_0 = 0.05$, $\epsilon_0 = 0.05$, $\epsilon_1 = 1$ and $\hat{\rho} - 3\hat{P} = 0.14$.

B. Numerical results

Using the full system of equations combining Einstein's equations and the Klein-Gordon equation, we have computed numerically the profile of the chameleon field, of the matter and of the geometry for two types of star configurations.

Before discussing these two cases, let us comment about a subtlety concerning the asymptotic behaviour of the geometry far from the star. In a realistic context, the star configuration should be matched asymptotically to a cosmological geometry, which is time dependent. Since we restrict our analysis to purely static configurations, we introduce instead some artificial matter which behaves like a cosmological constant far from the star. At large radius, the geometry thus approaches a Schwarzschild-de Sitter metric, which is static. We have checked that the details of the asymptotic matter do not modify the star configuration. Another possibility would be to introduce some non-trivial minimum in the chameleon potential.

1. Constant energy density stars

As a first (toy) example we considered a constant energy density star. In order to avoid unnecessary numerical difficulties connected with a sharp transition of the density from the star to the surrounding medium, we introduced the following smoothed profile for the density:

$$\hat{\rho}(\xi) = \frac{\hat{\rho}_c}{2} \left[1 - \tanh \left(\frac{\xi - 1}{\sigma} \right) \right] + \hat{\rho}_\infty, \quad (22)$$

where $\hat{\rho}_c$ is the rescaled density at the center of the star, $\hat{\rho}_\infty$ is the density of the surrounding medium far from the star and σ is a “smoothing” parameter (with values between 10^{-12} and 10^{-2}). It is easy to see, that for small enough σ the density is approximately equal to $\hat{\rho}_c$ for $\xi \lesssim 1$ and $\hat{\rho} \simeq \hat{\rho}_\infty$ for $\xi \gtrsim 1$, so that $\xi \simeq 1$ is the radius of the star. The boundary condition for the pressure is, $\hat{P}(\xi_2) = -\hat{\rho}_\infty$, so that we ensure that the de Sitter asymptotic behaviour is recovered for our numerical solution. In this case the pressure is found as a function of ξ , and \hat{P} inside the star depends on the boundary condition ξ_2 . This seemingly paradoxical situation is due to the artificial choice (22), but, as we have checked, the effect is tiny because the ratio between the star energy density and the asymptotic one is huge.

For a given coupling Q , the numerical system depends on three independent parameters: $\hat{\rho}_c$, v_0 and ϵ_0 , while $\hat{\phi}_\infty = 1/2$ and the rescaled asymptotic density ρ_∞ is determined by $\hat{\rho}_\infty = v_0 \epsilon_0 / Q$ according to (19). Since the backreaction of the scalar field on the star itself is very small, the compactness of the star depends only on the parameter $\hat{\rho}_c$. Consequently, for fixed parameters v_0 and ϵ_0 , increasing the central density leads to stars that are more and more compact, and therefore more and more relativistic. In Fig. 3, we plot the profile of the scalar field for stars with different central densities, corresponding to a gravitational potential ranging from 0.00168 to 0.165. As the central density increases, one sees how the scalar field profile evolves from a smooth configuration to a thin

shell configuration, where the scalar field abruptly jumps within a small range of radii. This is in agreement with the Newtonian result [19] that $\Delta r/r_* \approx (\phi_\infty - \phi_c)/(6QM_P\Phi_*) \approx \epsilon_0/(12Q\Phi_*)$.

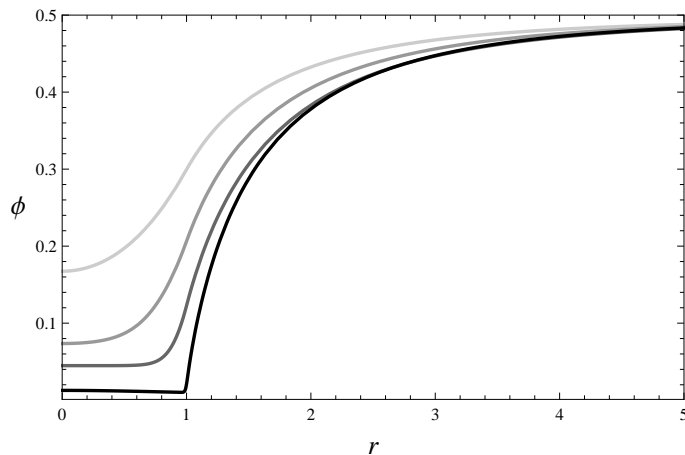


FIG. 3: Profiles of the scalar field ϕ (in Planck units) as a function of radius of the star (in units of $r_0 = M_P \hat{\rho}_c \tilde{\rho}_c^{1/2}$) for constant density stars with the equation of state (22). The parameters are chosen as follows, $\sigma = 0.01$, $Q = \epsilon_1 = 1$, $\epsilon_0 = v_0 = 0.01$, and the rescaled densities of the star are (from light gray to black), $\hat{\rho}_c = 0.01, 0.02, 0.05, 1$. The values of the gravitational potential at the surface of the star are, respectively, 0.00168, 0.00334, 0.0083 and 0.165. The increasing rescaled density corresponds to an increasing physical density while the physical radius of the star is being fixed.

Essentially the thin-shell solution can be understood as follows. The solution tries to minimize the sum of the potential energy and of the gradient energy, with the constraints that $\phi' = 0$ at $r = 0$ and ϕ fixed asymptotically. As the energy density in the star increases, to be away from the minimum of the effective potential becomes very costly energetically and, therefore, the field prefers to stay as much as possible close to its minimum. At some point close to the star radius, however, the field starts to move away from its effective minimum. In this region, the contribution from the potential on the right hand side of the Klein-Gordon equation becomes negligible with respect to the matter dependent term, and that the field “evolves” very quickly, driven by this “matter force” term. In the relativistic regime, analytical expressions describing the profile of the scalar field in the thin shell regime have been obtained in [26]: they apply to constant energy density stars and in the linearized approximation for the gravitational potential.

If one continues to increase the central energy density of the star, one ends up reaching the critical value for which $\hat{\rho} - 3\hat{P} < 0$ in the innermost central region of the star. The profile of the scalar field in the central region of the star is then radically altered, as one can see on Fig. 4, because there is no local minimum for the scalar field in this region.

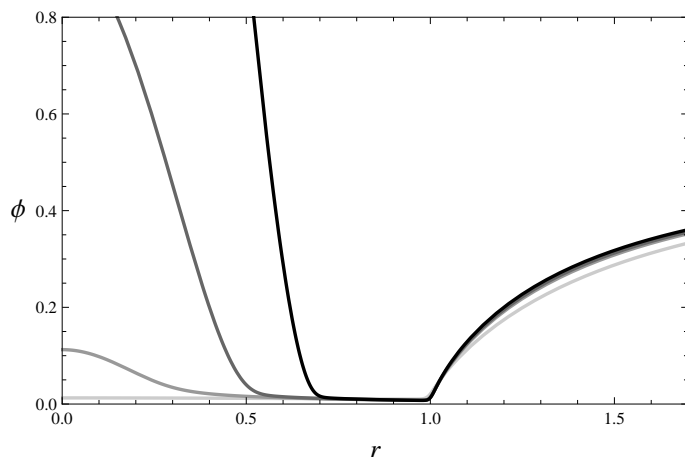


FIG. 4: Profiles of the scalar field ϕ (in Planck units) as a function of radius of the star (in units of $r_0 = M_P \hat{\rho}_c \tilde{\rho}_c^{1/2}$) for stars with $\hat{\rho} - 3\hat{P} < 0$ in the central region. The rescaled densities of the star (from light gray to black): $\hat{\rho}_c = 1, 1.7, 1.8, 1.9$. The other parameters are the same as in Fig. 3. The values of the gravitational potential at the surface of the star are, respectively, 0.165, 0.280, 0.298 and 0.318.

2. Thin shell effect

It is also instructive to see how much, depending on the density of the star, the geometry outside the star is close to that expected in general relativity. Numerically, one can estimate the post-Newtonian parameter $\tilde{\gamma}$ by comparing the coefficients of the terms in $1/r$ in the metric components \tilde{g}_{tt} and \tilde{g}_{rr} .

Since we work in the Einstein frame, let us first discuss the metric components g_{tt} and g_{rr} . One subtlety here is that the metric is asymptotically Schwarzschild-de Sitter rather than simply Schwarzschild and the asymptotic behaviours of the metric components are therefore

$$e^\nu \approx e^{-\lambda} \approx 1 - \frac{2GM}{r} - \frac{\Lambda}{3}r^2. \quad (23)$$

To estimate M numerically, we have subtracted from the metric components the cosmological constant term with

$$\Lambda = \rho_\infty e^{4Q\phi_\infty/M_P} + V_\infty,$$

where ϕ_∞ is the asymptotic minimum of the scalar field and $V_\infty \equiv V(\phi_\infty)$. We have checked that the two metric components, in the Einstein frame, provide the same value M . This means, in particular, that the backreaction due to the scalar field gradient is negligible outside the star.

In the Jordan frame, the metric components are $\tilde{g}_{\mu\nu} = \exp(2Q\phi/M_P)g_{\mu\nu}$. The asymptotic behaviour of the scalar field is of the form

$$\phi \approx \phi_\infty + 2\frac{GM}{r}Q_{\text{eff}}e^{-m_{\text{eff}}r},$$

where Q_{eff} is the effective coupling of the scalar field to the star, which is strongly suppressed in the thin shell regime. Combining this expression with (23), it is easy to get

$$\begin{aligned} \tilde{g}_{tt} &\approx e^{2Q\phi_\infty} \left[1 - 2(1 - 2QQ_{\text{eff}}) \frac{GM}{r} - \frac{\Lambda}{3}r^2 \right], \\ \tilde{g}_{rr}^{-1} &\approx e^{-2Q\phi_\infty} \left[1 - 2(1 + 2QQ_{\text{eff}}) \frac{GM}{r} - \frac{\Lambda}{3}r^2 \right], \end{aligned}$$

where, for simplicity, we have neglected the exponential decay. The effective $\tilde{\gamma}$ parameter is therefore

$$\tilde{\gamma} = \frac{1 - 2QQ_{\text{eff}}}{1 + 2QQ_{\text{eff}}}.$$

The general relativistic value, $\tilde{\gamma} = 1$, is thus recovered in the limit where the effective scalar charge Q_{eff} of the star is strongly suppressed, i.e. in the thin shell limit. This is illustrated in Fig. 5, where we have estimated numerically the effective coupling Q_{eff} as well as the post-Newtonian parameter $\tilde{\gamma}$ for stars with increasing energy density.

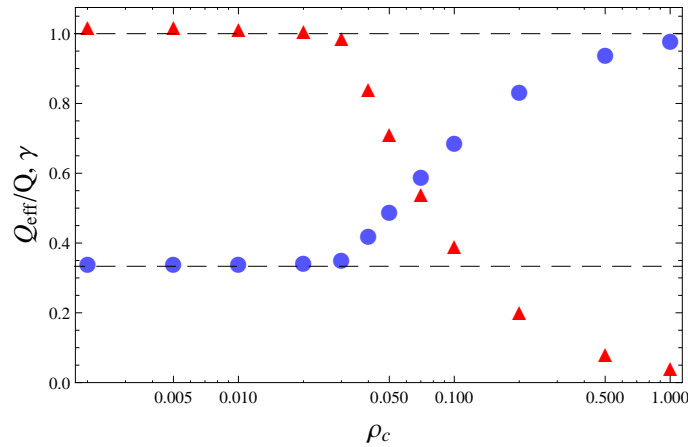


FIG. 5: Evolution of the numerical estimates for Q_{eff}/Q (red triangles) and for the post-newtonian parameter $\tilde{\gamma}$ (blue dots) as we increase the energy density of the star (constant energy density star). The “bare” coupling is here $Q = 1/2$, which corresponds to $\tilde{\gamma} = 1/3$ in the absence of screening. The other parameters are $\epsilon_0 = 10^{-2}$, $v_0 = 10^{-8}$ and $\xi_* = 1$.

3. Polytropic relativistic stars

Let us now consider relativistic stars with the more realistic equation of state (17). Although it is appropriate for the bulk of the star, it must be slightly modified at the edge of the star for the following reasons. First of all, the equation of state in Eq. (17) behaves like $\hat{P} \propto \hat{\rho}^2$ for small densities. This leads to pathologies, e. g. the ill-posed Cauchy problem for small fluctuations in the limit $\hat{\rho} \rightarrow 0$, as discussed in [27] in another context. Another reason is that the numerical calculations require a smooth transition between the star and the exterior matter.

We choose the following modification of the equation of state (17),

$$\hat{\rho} = \hat{P} + 2 \left(\frac{\hat{P} + \hat{\rho}_\infty}{2.24} \right)^{1/2}, \quad (25)$$

where we have introduced the (rescaled) asymptotic energy density $\hat{\rho}_\infty$, which is an extremely small parameter with respect to the pressure and energy density in the star. Note that for $\hat{P} \gtrsim \hat{\rho}_\infty$ the modified equation of state (25) comes to the original equation of state for the neutron star (17), while for small \hat{P} the modified equation of state allows the cosmological term behavior⁵. It is easy to see that for small $\hat{\rho}_\infty$ the “fluid” (25) is in the regime of a cosmological constant when $-\hat{P} = \hat{\rho} \simeq \hat{\rho}_\infty$.

Having specified the equation of state for the star and the surrounding matter (25), we also need to fix the boundary conditions. Apart from the four usual conditions (18), the boundary condition on the pressure is specified at the center of the star: $\hat{P}(0) \simeq 0.286$ (which corresponds to a realistic value, in the rescaled units). It is interesting to note, that the system “chooses” by itself the cosmological term-like behavior asymptotically, $\hat{P} = -\hat{\rho}$, we do require any conditions on the density nor the pressure at the infinity. This situation is in contrast to the constant density star configuration, where we imposed the “correct” asymptotic behavior at infinity specifying the boundary condition for \hat{P} .

The numerical solution for the scalar field profile is shown in Fig. 6 for the parameters $Q = \epsilon_1 = 1$, $\epsilon_0 = 0.01$, $v_0 = 0.01$, $\rho_0 = 10^{-4}$. The minimum of the effective potential is indicated by a dashed line. In the central part of the star, the scalar field strictly follows this minimum. Note that, as the radius increases, the minimum first increases and then decreases. This non-monotonous evolution is the consequence of the non-monotonous evolution of the quantity $\tilde{\rho} - 3\tilde{P}$, which was pointed previously. Slightly before reaching the radius of the star (delimited by the quasi-vertical dashed line), the scalar field starts to move away from its minimum, with a steep gradient, and asymptotically evolves toward its asymptotic minimum far from the star.

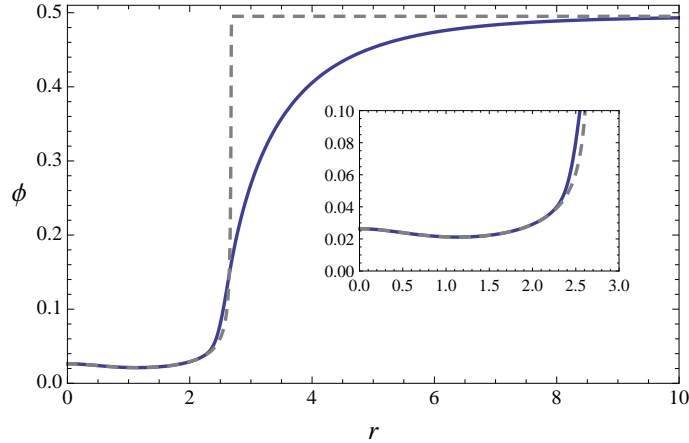


FIG. 6: Profile for the scalar field ϕ (in Planck units), shown by solid (blue) line, as a function of the radius (in units of $r_0 = M_P \tilde{\rho}_c^{-1/2}$), for the equation of state (25) with $\epsilon_0 = 0.01$, $v_0 = 0.01$ and $\hat{\rho}_\infty = 10^{-4}$. The value of the gravitation potential, $\hat{\mathcal{M}}(\xi)/\xi$, at the surface of the star is 0.252. The value ϕ_{\min} for the minimum of the effective potential is plotted by dashed (gray) line.

⁵ In fact, our numerical integration shows that the system settles down at the cosmological term, $\hat{P} = -\hat{\rho}$, at large ξ .

IV. $f(R)$ GRAVITY

We now turn to $f(R)$ gravity, restricting ourselves to the conventional metric formulation. Some of our results on relativistic stars have already appeared in a separate publication [7]. Here, we present more details and stress the strong analogy of these models with the chameleon models.

A. The models

The $f(R)$ models are usually described by an action of the form

$$S = \frac{M_P^2}{2} \int d^4x \sqrt{-\tilde{g}} f(\tilde{R}) + S_m[\Phi_m; \tilde{g}_{\mu\nu}], \quad (26)$$

where the matter is minimally coupled to the metric $\tilde{g}_{\mu\nu}$, with corresponding Ricci tensor $\tilde{R}_{\mu\nu}$ and scalar curvature \tilde{R} . It is convenient to reexpress f in the form

$$f(\tilde{R}) = R_0 \mathcal{F}(x), \quad x \equiv \frac{\tilde{R}}{R_0}$$

where \mathcal{F} is a dimensionless function and R_0 is some parameter.

In contrast with many papers on $f(R)$ theories, in particular [5] and [6], we choose here to reexpress the model as a scalar- tensor theory in the so-called Einstein frame. The two formulations are of course equivalent (at least at the classical level), but the Einstein frame is useful to compare directly the behaviour of $f(R)$ theories with that of chameleon models, discussed in the previous section.

By introducing the scalar field

$$\phi = \sqrt{\frac{3}{2}} M_P \ln f_{,\tilde{R}} = \sqrt{\frac{3}{2}} M_P \ln \mathcal{F}'(x) \quad (27)$$

and the metric

$$g_{\mu\nu} = \Omega^{-2} \tilde{g}_{\mu\nu}, \quad \Omega^{-2} = f_{,\tilde{R}} = \exp\left[\sqrt{\frac{2}{3}} \phi / M_P\right]$$

the action (26) can be reexpressed in the form (1) with the coupling

$$Q = -1/\sqrt{6},$$

and the potential

$$V = M_P^2 \frac{\tilde{R} f_{,\tilde{R}} - f}{2 f_{,\tilde{R}}^2}, \quad (28)$$

which can be expressed in terms of ϕ by inverting the definition (27) of ϕ as a function of \tilde{R} .

Note that, in contrast to the chameleon case discussed in the previous section, the coupling Q is here negative. We could have chosen a positive value by changing the sign of ϕ , but we have kept the usual convention. When comparing the results of this section with the previous one, it is useful to keep in mind that the signs of Q and ϕ can be simultaneously changed.

The function $f(R)$ is severely constrained by observations. For the present discussion, we focus our attention on the specific class of models introduced by Starobinsky [4],

$$f(\tilde{R}) = R_0 \left[x - \lambda \left(1 - (1 + x^2)^{-n} \right) \right], \quad x \equiv \frac{\tilde{R}}{R_0}. \quad (29)$$

The asymptotic de Sitter solution $\tilde{R}_\infty \equiv x_\infty R_0$ corresponds to a minimum of V and depends on the parameter λ . For practical purposes, it is simpler to choose x_∞ as the parameter and then express λ as a function x_∞ , with the restriction that x_∞ must be chosen such that it corresponds to a stable minimum of the potential. Details and explicit expressions can be found in the appendix. The potential for the scalar field in the model with $n = 1$ and $x_\infty = 3.6$ is plotted in Fig. 7.

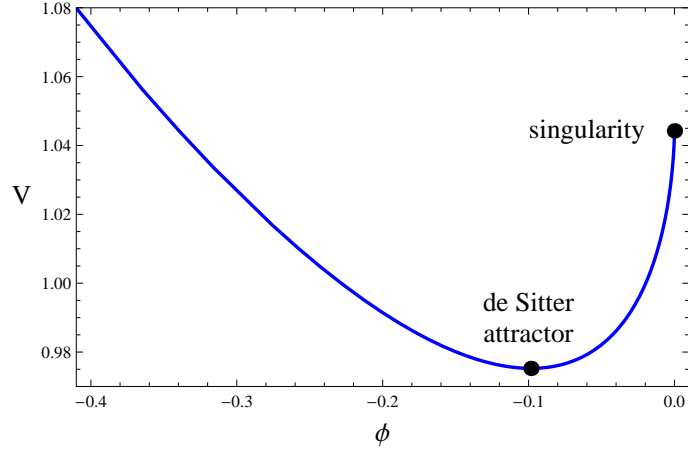


FIG. 7: Potential V (in units of $M_P^2 R_0$) as a function of ϕ (in Planck units) for $n = 1$ and $x_\infty = 3.6$. The lower black dot corresponds to the de-Sitter attractor while the upper-right dot shows the curvature singularity.

B. High curvature regime

Inside the star, the curvature is much higher than the cosmological curvature R_0 , i.e. $x \gg 1$. It is instructive to consider the asymptotic expansion of the potential and its derivatives in order to understand intuitively the behaviour of the scalar field, noting that the infinite curvature limit corresponds to $\phi \rightarrow 0^-$.

Using the asymptotic expansion

$$\mathcal{F}(x) \simeq x - \lambda + \lambda x^{-2n}, \quad (x \gg 1), \quad (30)$$

one finds

$$\mathcal{V}(x) \simeq \frac{\lambda}{2} [1 - (1 + 2n)x^{-2n}],$$

which shows that the amplitude of the potential remains *finite* when $x \gg 1$, i.e. when ϕ approaches 0. This is quite different from the chameleon model discussed in the previous section and this can cause some worry that the singularity can be easily accessible for high enough curvatures, as discussed in [5].

However, the derivative of the potential still goes to infinity in this limit and this property prevents the scalar field to reach the singularity. Indeed, the derivative of the effective potential is given by (see appendix)

$$\frac{dV_{\text{eff}}}{d\phi} \simeq \sqrt{\frac{2}{3}} M_P R_0 \frac{x}{2} - \frac{1}{\sqrt{6} M_P} (\tilde{\rho} - 3\tilde{P}),$$

which implies the existence of a minimum

$$x_{\min} \simeq \frac{\tilde{\rho} - 3\tilde{P}}{M_P^2 R_0}, \quad \phi_{\min} = -\sqrt{6} \lambda n x_{\min}^{-2n-1}. \quad (31)$$

at least if the matter term $\tilde{\rho} - 3\tilde{P}$ is positive. It can be checked that this is indeed a minimum by computing the second derivative of the effective potential. This leads to a positive effective square mass (see appendix),

$$m_{\text{eff}}^2 \simeq R_0 \frac{x_{\min}^{2n+2}}{6\lambda n(2n+1)},$$

which becomes very large at high curvature.

As the energy density in the star increases toward the center, one expects that the scalar field will be closer and closer to the singularity (without reaching it however), simply because the minimum of the effective potential is closer and closer to the singularity. This is confirmed by our numerical calculations, which we discuss below.

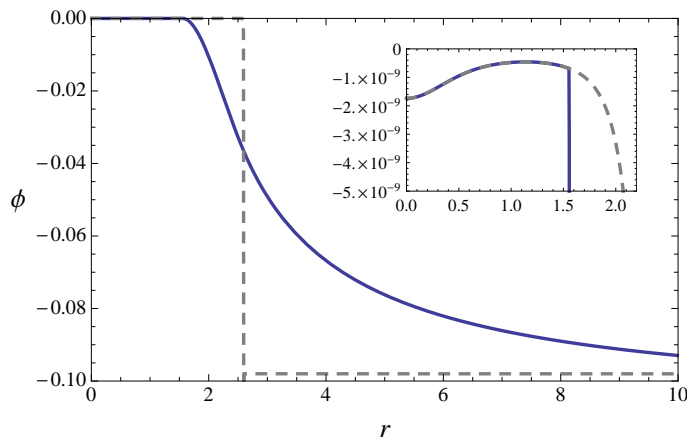


FIG. 8: Profile of the scalar field ϕ (in Planck units), shown by solid (blue) line, as a function of the radius (in units of $M_P \bar{\rho}_c^{-1/2}$), for the model (29) with $n = 1$, $x_\infty = 3.6$ (see appendix for the definition of x_∞) and $v_0 = 10^{-4}$. The value ϕ_{\min} for the minimum of the effective potential is plotted by dashed (gray) line.

C. Numerical results

We have integrated numerically the system of equations (15), together with (11), for Starobinsky's model (29) with $n = 1$. Our parameters are $\epsilon_0 = \epsilon_1 = 1$ and the rescaled potential is

$$\hat{V} = v_0 \mathcal{V}, \quad v_0 = r_0^2 R_0 = \frac{M_P^2 R_0}{\bar{\rho}_c},$$

where the explicit expression for \mathcal{V} in the case $n = 1$ is given by (A6) in the appendix.

Here, the parameter v_0 corresponds to the ratio between the energy density at infinity (i.e. the cosmological energy density) and the energy density at the center of the star. Realistic values of this parameter are thus extremely small, typically $v_0 \sim 10^{-40}$, and are numerically challenging to reach, because the scalar field value at the center is proportional to v_0^3 , as can be seen by comparing the definition of v_0 with the minimum defined in (31) in the case $n = 1$. The smallest value we considered is $v_0 = 10^{-4}$, which is much higher than the realistic one. However we believe that the situation is qualitatively similar for smaller values.

The profile of the scalar field inside and outside the star is plotted in Fig. 8. As is clear from the figure, the scalar field tends to interpolate between an extremely high density regime, inside the star, and a very low density regime, outside the star. This behaviour is quite analogous to that of the chameleon model discussed in the previous section and the solution that we obtain is analogous to the thin-shell solution. What differs from the usual chameleon models is the presence of the singularity. In the very high density regime, the scalar field is very close to the singularity because the minimum of the effective potential is itself very close to the singularity. To give an analogy, it is like the scalar field is following a track very near a precipice, but because the effective mass is very high in this regime, the scalar field is securely attached to the track and does not fall into the nearby precipice.

These numerical results, previously presented in [7], contradict the results of [6], where it was claimed that stars with a gravitational potential larger than a critical value $\Phi_{\max} \approx 0.1$ could not be constructed. The reason advocated in [6] was the presence of the singularity, as stressed previously in [5]. However, as we showed in [7], the analytical arguments in [5] and [6] supporting this interpretation were not valid⁶. We also indicated that the exploration of the scalar field profile was numerically challenging for small values of v_0 , because the distance between the scalar field value and the singularity is proportional to v_0^3 . Since the value used in [6] was $v_0 \sim 10^{-6}$, one could strongly suspect that the results obtained in [6] were probably due to a numerical instability. This explanation was confirmed subsequently in [28], which tried to reproduce the numerical analysis as [6], using the same technique, namely the shooting method. Indeed, they were able to construct highly relativistic stars, but with a parameter $v_0 \sim 10^{-2}$.

Although we show only our numerical results in the case of the polytropic equation of state, we have also performed similar numerical integrations for constant energy density stars. We have obtained quite similar results as in the

⁶ Note also that, obviously, the problem encountered in [6] cannot be explained by the sign of the trace of the energy-momentum tensor since their gravitational potential is well below the critical value (10).

chameleon model. For instance, we have been able to obtain numerical solutions up to the value $\Phi_* = 0.33$ for the gravitational potential ⁷ (with the parameters $\epsilon_1 = \epsilon_0 = 1$, $v_0 = 0.01$).

D. “Cured” $f(R)$ gravity

Although the existence of neutron stars is, so far⁸, compatible with the $f(R)$ models we have just investigated, the situation is not the same in cosmology. It has indeed been noticed in [4, 29, 30] that the behaviour of these theories is pathological when one considers their past cosmological evolution, with the generic presence of a singularity in the not so distant past. As a way to “cure” this pathology at high curvature, it has been suggested to add R^2 term⁹. This extra term radically changes the behaviour of the potential at very high curvature, as illustrated in Fig. 9 for the model

$$f(\tilde{R}) = R_0 \left[x - \lambda \left(1 - (1 + x^2)^{-n} \right) + \sigma x^2 \right], \quad x \equiv \frac{\tilde{R}}{R_0}. \quad (32)$$

One sees that the corresponding potential has no singularity at $\phi = 0$ and the scalar field can now take positive values, corresponding to high curvatures.

The extra R^2 term has the additional advantage that it can drive inflation in the early Universe (see e.g. [33, 34]), as in the pioneering Starobinsky model [35]. Recently, however, it was argued in [13] that one cannot relate smoothly the inflation epoch with the present acceleration epoch with the above model (32). As an example of a viable transition between two accelerating solutions, the model

$$f(\tilde{R}) = (1 - c)\tilde{R} + c\epsilon \ln \left[\frac{\cosh(\tilde{R}/\epsilon - b)}{\cosh b} \right] + \frac{\tilde{R}^2}{6M^2}, \quad \epsilon \equiv \frac{R_0}{b + \ln(2 \cosh b)} \quad (33)$$

with $0 < c < 1/2$, was proposed in [13], where the new mass scale M must be of the order 10^{12} GeV to reproduce the standard predictions of inflation. In the high curvature regime ($R \gg R_0$), one finds

$$f(\tilde{R}) \approx \tilde{R} - cR_0 + c\epsilon e^{2b} e^{-2\tilde{R}/\epsilon} + \frac{\tilde{R}^2}{6M^2}.$$

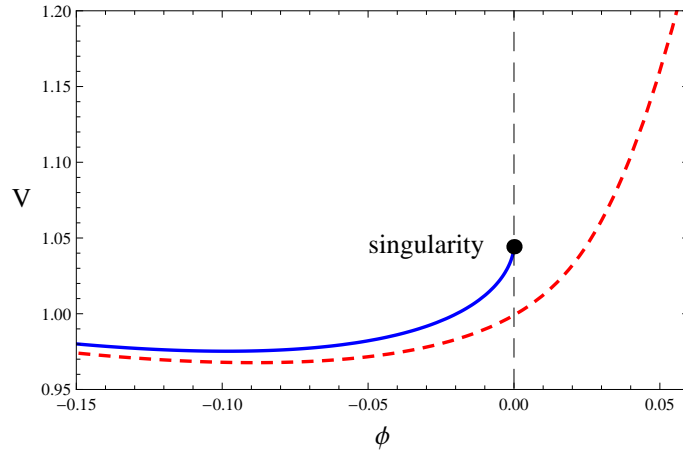


FIG. 9: Potential V (in units of $M_P^2 R_0$) as a function of ϕ (in Planck units) for $n = 1$ and $x_\infty = 3.6$. The blue curve corresponds to the original Starobinsky cosmological model with the curvature singularity at $\phi = 0$. The red curve represents the “cured” Starobinsky model with $\sigma = 10^{-3}$.

⁷ Note that a similar value for the maximum gravitational potential, $\Phi_* = 0.345$, was obtained in [28].

⁸ It would be also worth considering a supernova explosion and the birth of a neutron star in the context of $f(R)$ theories. The present work deals only with static solutions and not how they could be reached in an evolutionary process.

⁹ Another way to avoid a pathological behavior would be to construct $f(R)$ model separating the singularity with infinite energy barrier, as it was done in [31]. It was argued, however, that this particular model does not satisfy local gravity constraints and SDSS data [32].

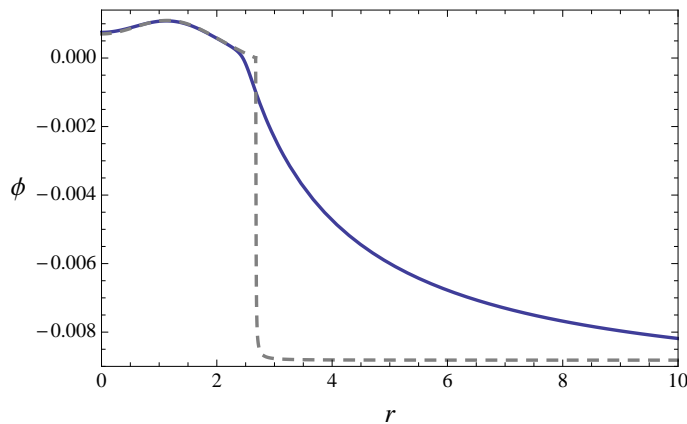


FIG. 10: Profile of the scalar field in the model (33) with the parameters $\sigma = 2 \times 10^{-6}$, $c = 0.4$, $b = 4$, $v_0 = 10^{-3}$.

The interior of a neutron star corresponds to the high curvature regime, but the curvature is many orders of magnitude smaller than M^2 . In this intermediate regime $R_0 \ll \tilde{R} \ll M^2$, the scalar field behaves like

$$\frac{\phi}{M_P} = \sqrt{\frac{3}{2}} \ln f_{,\tilde{R}} \approx \sqrt{\frac{3}{2}} \left[-2c e^{2b} e^{-2\tilde{R}/\epsilon} + \frac{\tilde{R}}{3M^2} \right]. \quad (34)$$

The two terms on the right hand side are extremely small. However, the first term decays exponentially as the curvature increases and the second term will typically dominate at the center of a neutron star.

We plot on Fig. 10 the profile of the scalar field in this model with small values for v_0 and $\sigma = R_0/(6M^2)$, although not small enough to be realistic. Once again, we observe that the scalar field follows the minimum of its effective potential in the core of the star. Near the boundary of the star, it deviates from the local minimum and converges towards the asymptotic minimum outside the star. The scalar field is negative deep inside the star because the second term on the right hand side of (34) dominates, whereas it is positive near the boundary and outside the star.

V. DISCUSSION AND CONCLUSION

We have studied in this work relativistic stars in scalar tensor and $f(R)$ theories that use the chameleon mechanism. The behaviour of the scalar field is extremely similar in the two types of models. The main properties are the following.

Deep inside the star, the scalar field follows very closely the minimum of its effective potential (if it exists). As a consequence, if the minimum changes as a function of the radius, the scalar field will faithfully follow it. If $\tilde{\rho} - 3\tilde{P} < 0$, which can occur for instance in the central region of very compact stars with constant energy density, there is no minimum for the effective potential. It is however possible to find numerical solutions for constant energy stars with both $w < 1/3$ and $w > 1/3$ regions, but only up to some maximum gravitational potential. We have given qualitative arguments to show that one expects tachyonic instabilities if most of the star is characterized by $w > 1/3$.

As already emphasized in our previous work [7], our results invalidate the claim that highly relativistic stars cannot be constructed in $f(R)$ theories. Numerically, the construction of a relativistic stars in $f(R)$ gravity is a challenging task because the scalar field value is extremely close to the singularity in the center of the star. We have also constructed relativistic stars in the so-called “cured” $f(R)$ models, which have been advocated to solve a cosmological singularity problem.

We have also illustrated how the screening effect of the chameleon mechanism manifests itself for relativistic stars, by computing numerically the effective coupling of the star as well as the post-Newtonian parameter $\tilde{\gamma}$.

Note: while this paper was being completed, another paper [36] on relativistic stars in $f(R)$ theories appeared on the arXiv, although in a different context.

Acknowledgments

We would like to thank Nathalie Deruelle, Gilles Esposito-Farese, Andrei Frolov, Ericourgoulhon, Kei-ichi Maeda, Jérôme Novak, Ignacy Sawicki, Alexei Starobinsky, Shinji Tsujikawa and Riad Ziour for very instructive discussions. The work of E.B. was supported by the EU FP6 Marie Curie Research and Training Network UniverseNet (MRTN-CT-2006-035863).

APPENDIX A

1. General formulas for $f(R)$ models

For $f(\tilde{R})$ models, the potential V , introduced in (28), can be written as

$$V = M_P^2 \frac{\tilde{R}f_{,\tilde{R}} - f}{2f_{,\tilde{R}}^2} = M_P^2 R_0 \mathcal{V}(x), \quad \mathcal{V}(x) \equiv \frac{x\mathcal{F}'(x) - \mathcal{F}(x)}{2\mathcal{F}'(x)^2}, \quad (\text{A1})$$

where $f(\tilde{R}) = R_0 \mathcal{F}(x)$ and $x \equiv \tilde{R}/R_0$. The associated scalar field is defined by

$$\phi = \sqrt{\frac{3}{2}} M_P \ln f_{,\tilde{R}} = \sqrt{\frac{3}{2}} M_P \ln \mathcal{F}'(x) \quad (\text{A2})$$

Combining (A1) and (A2), one finds for the first and second derivatives of the potential V in terms of ϕ the following expressions:

$$\frac{dV}{d\phi} = \sqrt{\frac{2}{3}} M_P \frac{2f - \tilde{R}f_{,\tilde{R}}}{2f_{,\tilde{R}}^2}, \quad (\text{A3})$$

$$\frac{d^2V}{d\phi^2} = \frac{1}{3f_{,\tilde{R}\tilde{R}}} \left[1 + \frac{\tilde{R}f_{,\tilde{R}\tilde{R}}}{f_{,\tilde{R}}} - \frac{4ff_{,\tilde{R}\tilde{R}}}{f_{,\tilde{R}}^2} \right]. \quad (\text{A4})$$

2. Starobinsky's models

Let us now restrict ourselves to the specific class of models introduced by Starobinsky[4],

$$f(\tilde{R}) = R_0 \left[x - \lambda \left(1 - (1 + x^2)^{-n} \right) \right], \quad x \equiv \frac{\tilde{R}}{R_0}.$$

Substituting this expression into (A3) and solving $V' = 0$ yields the minimum of V corresponding to the asymptotic de Sitter solution $\tilde{R}_\infty \equiv x_\infty R_0$. It is convenient to express the parameter λ in terms of x_∞ :

$$\lambda = \frac{x_\infty(1 + x_\infty^2)^{n+1}}{2[(1 + x_\infty^2)^{n+1} - 1 - (n+1)x_\infty^2]}.$$

In terms of x_∞ , the minimum of the potential is given by

$$V_\infty = V(\phi_\infty) = \frac{1}{4} M_P^2 R_0 x_\infty \frac{(1 + x_\infty^2)^{n+1} - 1 - (n+1)x_\infty^2}{(1 + x_\infty^2)^{n+1} - 1 - (2n+1)x_\infty^2}$$

for

$$\phi_\infty = \sqrt{\frac{3}{2}} M_P \ln \left[1 - \frac{nx_\infty^2}{(1 + x_\infty^2)^{n+1} - 1 - (n+1)x_\infty^2} \right].$$

At the minimum, the effective squared mass is

$$m_\infty^2 = \frac{d^2V}{d\phi^2}(\phi_\infty) = \frac{4V_\infty}{M_P^2} \frac{[(x_\infty^2 + 1)^{n+2} - (2n^2 + 3n + 1)x_\infty^4 - (n+2)x_\infty^2 - 1]}{3nx_\infty^2[(2n+1)x_\infty^2 - 1]}.$$

The parameter x_∞ must be chosen so that $m_\infty^2 > 0$.

Let us now consider the regime where the curvature is much higher than the cosmological curvature R_0 , i.e. $x \gg 1$. In this regime,

$$f(\tilde{R}) \simeq R_0 (x - \lambda + \lambda x^{-2n}), \quad (\text{A5a})$$

$$f'(\tilde{R}) \simeq 1 - 2\lambda n x^{-2n-1}, \quad (\text{A5b})$$

$$f''(\tilde{R}) \simeq \frac{2}{R_0} \lambda n(2n+1) x^{-2n-2}, \quad (\text{A5c})$$

and the scalar field behaves like

$$\sqrt{\frac{2}{3}} \frac{\phi}{M_P} \simeq -2\lambda n x^{-2n-1} \quad (x \gg 1).$$

Substituting in (A3) the above expressions, one finds that the derivative of the effective potential, whose general expression can be found in (13), is given by

$$\frac{dV_{\text{eff}}}{d\phi} \simeq \sqrt{\frac{2}{3}} M_P R_0 \frac{x}{2} - \frac{1}{\sqrt{6} M_P} (\tilde{\rho} - 3\tilde{P}) \quad (x \gg 1).$$

The minimum of the effective potential is thus determined by

$$x_{\text{min}} \simeq \frac{\tilde{\rho} - 3\tilde{P}}{M_P^2 R_0},$$

and exists only if the matter term $\tilde{\rho} - 3\tilde{P}$ is positive. Substituting in (A4) the expressions (A5), one also finds that the effective mass at the minimum behaves like

$$m_{\text{eff}}^2 \approx \frac{R_0}{6\lambda n(2n+1)} x_{\text{min}}^{2n+2}.$$

In the particular case $n = 1$, one can invert the relation between ϕ and \tilde{R} and obtain an explicit formula expressing x as a function of ϕ , which we do not write down because it is rather ugly. Substituting this relation

$$\mathcal{V}(x) = \frac{\lambda (x^2 - 1) (x^3 + x)^2}{2 (x^4 + 2x^2 - 2\lambda x + 1)^2} \quad (\text{A6})$$

thus gives an explicit expression for the potential as a function of ϕ .

-
- [1] T. P. Sotiriou and V. Faraoni, arXiv:0805.1726 [gr-qc].
 - [2] W. Hu and I. Sawicki, Phys. Rev. D **76**, 064004 (2007) [arXiv:0705.1158 [astro-ph]].
 - [3] S. A. Appleby and R. A. Battye, Phys. Lett. B **654**, 7 (2007) [arXiv:0705.3199 [astro-ph]].
 - [4] A. A. Starobinsky, JETP Lett. **86**, 157 (2007) [arXiv:0706.2041 [astro-ph]].
 - [5] A. V. Frolov, Phys. Rev. Lett. **101**, 061103 (2008) [arXiv:0803.2500 [astro-ph]].
 - [6] T. Kobayashi and K. i. Maeda, Phys. Rev. D **78**, 064019 (2008) [arXiv:0807.2503 [astro-ph]].
 - [7] E. Babichev and D. Langlois, arXiv:0904.1382 [gr-qc].
 - [8] K. Kainulainen, J. Piilonen, V. Reijonen and D. Sunhede, Phys. Rev. D **76**, 024020 (2007) [arXiv:0704.2729 [gr-qc]].
 - [9] M. C. B. Abdalla, S. Nojiri and S. D. Odintsov, Class. Quant. Grav. **22**, L35 (2005) [arXiv:hep-th/0409177].
 - [10] S. Capozziello, M. De Laurentis, S. Nojiri and S. D. Odintsov, Phys. Rev. D **79** (2009) 124007 [arXiv:0903.2753 [hep-th]].
 - [11] A. Dev, D. Jain, S. Jhingan, S. Nojiri, M. Sami and I. Thongkool, Phys. Rev. D **78** (2008) 083515 [arXiv:0807.3445 [hep-th]].
 - [12] I. Thongkool, M. Sami, R. Gannouji and S. Jhingan, Phys. Rev. D **80** (2009) 043523 [arXiv:0906.2460 [hep-th]].
 - [13] S. Appleby, R. Battye and A. Starobinsky, arXiv:0909.1737 [astro-ph.CO].
 - [14] T. Damour and G. Esposito-Farese, Phys. Rev. Lett. **70**, 2220 (1993).
 - [15] T. Damour and G. Esposito-Farese, Class. Quant. Grav. **9**, 2093 (1992).
 - [16] B. Bertotti, L. Iess and P. Tortora, Nature **425** (2003) 374.
 - [17] G. Esposito-Farese, arXiv:0905.2575 [gr-qc].
 - [18] J. Khoury and A. Weltman, Phys. Rev. Lett. **93**, 171104 (2004) [arXiv:astro-ph/0309300].

- [19] J. Khoury and A. Weltman, Phys. Rev. D **69**, 044026 (2004) [arXiv:astro-ph/0309411].
- [20] T. Chiba, Phys. Lett. B **575**, 1 (2003) [arXiv:astro-ph/0307338].
- [21] I. Navarro and K. Van Acoleyen, JCAP **0702**, 022 (2007) [arXiv:gr-qc/0611127].
- [22] T. Faulkner, M. Tegmark, E. F. Bunn and Y. Mao, Phys. Rev. D **76**, 063505 (2007) [arXiv:astro-ph/0612569].
- [23] P. Brax, C. van de Bruck, A. C. Davis and D. J. Shaw, Phys. Rev. D **78**, 104021 (2008) [arXiv:0806.3415 [astro-ph]].
- [24] T. Harada, Prog. Theor. Phys. **98**, 359 (1997) [arXiv:gr-qc/9706014].
- [25] J. M. Lattimer and M. Prakash, Phys. Rept. **442**, 109 (2007) [arXiv:astro-ph/0612440].
- [26] S. Tsujikawa, T. Tamaki and R. Tavakol, JCAP **0905**, 020 (2009) [arXiv:0901.3226 [gr-qc]].
- [27] E. Babichev, V. Mukhanov and A. Vikman, JHEP **0802** (2008) 101 [arXiv:0708.0561 [hep-th]].
- [28] A. Upadhye and W. Hu, Phys. Rev. D **80**, 064002 (2009) [arXiv:0905.4055 [astro-ph.CO]].
- [29] S. Tsujikawa, Phys. Rev. D **77**, 023507 (2008) [arXiv:0709.1391 [astro-ph]].
- [30] S. A. Appleby and R. A. Battye, JCAP **0805**, 019 (2008) [arXiv:0803.1081 [astro-ph]].
- [31] V. Miranda, S. E. Joras, I. Waga and M. Quartin, Phys. Rev. Lett. **102** (2009) 221101 [arXiv:0905.1941 [astro-ph.CO]].
- [32] A. de la Cruz-Dombriz, A. Dobado and A. L. Maroto, Phys. Rev. Lett. **103** (2009) 179001 [arXiv:0910.1441 [astro-ph.CO]].
- [33] S. Nojiri and S. D. Odintsov, Phys. Lett. B **657**, 238 (2007) [arXiv:0707.1941 [hep-th]].
- [34] S. Nojiri and S. D. Odintsov, Phys. Rev. D **77**, 026007 (2008) [arXiv:0710.1738 [hep-th]].
- [35] A. A. Starobinsky, Phys. Lett. B **91**, 99 (1980).
- [36] A. Cooney, S. DeDeo and D. Psaltis, arXiv:0910.5480 [astro-ph.HE].